PositiveAssist: Energy-Gated Control for Positive Power Assistance of Exoskeleton in Walking, Running, and Stair Climbing

Juncheng Zhou, Weibo Gao, *Graduate Student Member, IEEE*, Jin Sen Huang, Kurt Lin, Wanqi Wu, and Hao Su, *Senior Member, IEEE*

***Abstract*—Assistance timing is a critical factor in exoskeleton control. This article introduces the energy-gated controller, which uses only two thigh-mounted inertial measurement units to estimate hip kinematics and predicted mechanical power so that assistive torque is delivered primarily during positive work phases. Our proposed method combines a power-based gating mechanism with a biomechanics-informed torque synthesis strategy that reconstructs extension assistance from a delayed flexion profile, without gait-phase detection or task-specific mode switching. Experimental results from six participants ($n = 6$) show that using a single fixed parameter set selected a priori, over $97.8\% \pm 1.2\%$ of delivered mechanical power remained positive during walking and above $94.8\% \pm 1.6\%$ during running, across 0.75–3.5 $\mathrm{m/s}$ without parameter retuning. Under the same fixed parameters, the controller was further tested in five overground nonperiodic locomotion tasks and showed smooth assistance during the tested gait transitions, indicating potential for real-world deployment.**

***Index Terms*—Energy-gated control, wearable robotics.**

I. Introduction

ACTIVE lower limb exoskeletons have demonstrated benefits in rehabilitation [1], [2] and mobility assistance [3], [4]. By delivering joint torque during locomotion, these devices can provide meaningful mechanical assistance [5], [6]. However, achieving timely and nonresistive assistance remains challenging under widely varying locomotor conditions [7]. Across both rhythmic (steady state) and nonrhythmic (transitional) motions and across users, the coordination between human motion and exoskeleton actuation becomes difficult to maintain [8]. In such situations, exoskeleton-induced resistance and negative mechanical work are associated with reduced comfort and user acceptance [9].

A broad class of lower limb exoskeleton controllers generate assistive torque based on kinematic signals that reflect the rhythmic structure of human gait. Finite state machine (FSM)-based methods segment gait events and apply phase-specific assistance [10], while oscillator-based methods track continuous gait cycles to schedule assistance [11]. These approaches are well-suited for cyclic locomotion when gait patterns remain consistent. Delayed output feedback control (DOFC) generates assistance by feeding back joint kinematics through a fixed phase delay and can support noncyclic movements [12]. The delay denotes a temporal offset between measured joint kinematics and the resulting assistive torque command, used to align assistance with biomechanically meaningful phases of motion while compensating for perception actuation latency. However, operation across different speeds or locomotion modes typically requires task-specific or speed-specific parameter tuning [13], which increases manual configuration and limits deployment simplicity.

Another broad class of approaches seeks to adapt assistance across activities and subjects through optimization or learning. Human-in-the-loop methods tune control parameters based on physiological measurements to individualize assistance [1], but depend on specialized sensing equipment. Recent learning-based methods train policies in simulation and have shown promising cross-condition adaptability [14], [15], [16], [17], but rely on deep neural networks for real-time inference. A comparison of representative lower limb exoskeleton control paradigms is summarized in Table I.

In collaborative robotic arms, interaction is commonly regulated through power-limiting and force-limiting mechanisms that enforce bounded or unidirectional energy exchange [18], [19]. These strategies guarantee safe physical interaction by preventing the robot from injecting harmful mechanical energy, effectively acting as energy-based safety filters during human–robot interaction. In these systems, however, human motion is

Received 15 January 2026; revised 30 March 2026; accepted 27 April 2026. Recommended by Technical Editor S. Kumar Mohan and Senior Editor Z. Sun. This work was supported in part by NSF CPS under Grant 2344956, in part by GCR under Grant 2524088, in part by CAREER under Grant 1944655, and in part by NIH under Grant 1R01EB035404-01. *(Corresponding author: Hao Su.)*

Juncheng Zhou, Weibo Gao, Jin Sen Huang, Kurt Lin, and Wanqi Wu are with the Lab of Biomechatronics and Intelligent Robotics, Department of Biomedical Engineering, New York University, New York, NY 11201 USA.

Hao Su is with the Lab of Biomechatronics and Intelligent Robotics, Department of Biomedical Engineering, New York University, New York, NY 11201 USA, and also with the Courant Institute School of Mathematics, Computing, and Data Science, New York University, New York, NY 10012 USA (e-mail: hao.su@nyu.edu).

This article has supplementary material provided by the authors and color versions of one or more figures available at https://doi.org/10.1109/TMECH.2026.3691108.

Digital Object Identifier 10.1109/TMECH.2026.3691108

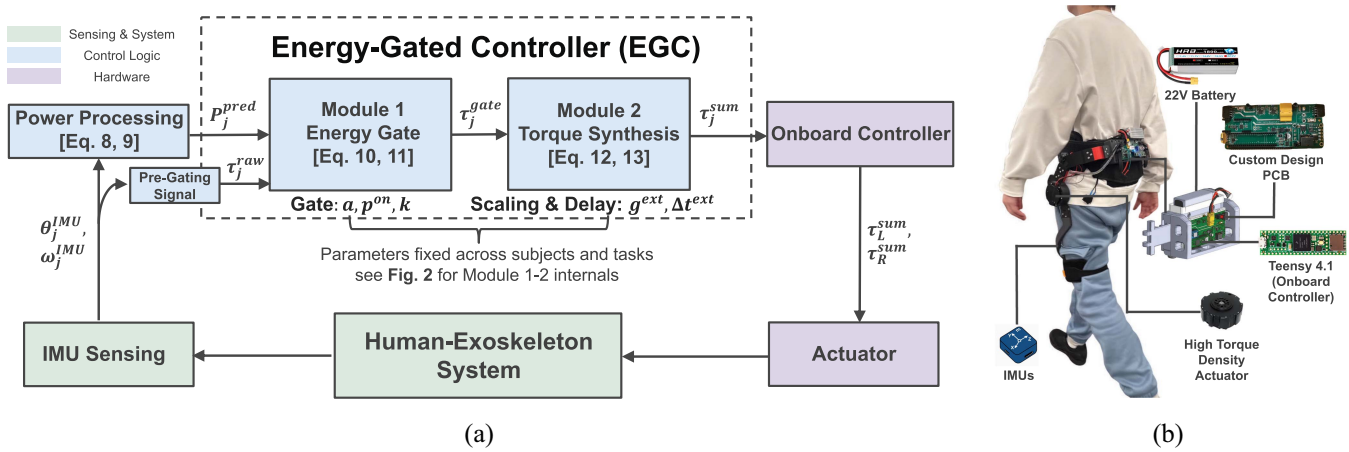

Fig. 1. Overview of the proposed EGC. (a) System-level control pipeline. Using IMU signals as inputs*, EGC estimates hip kinematics and processes joint mechanical power to coordinate two modules. Module 1 (energy gate) enables actuation only during positive-work intervals, while Module 2 (torque synthesis) reconstructs full-cycle assistance from a delayed and scaled flexion profile. Five physically interpretable parameters are selected a priori and fixed across all subjects and tasks in this study. (b) Experimental hip-exoskeleton platform. A compact hip exoskeleton supports real-time implementation for continuous walking, running, and stair climbing without parameter retuning [20]. *IMU inputs are sagittal-plane thigh angles and angular velocities.

TABLE I
COMPARISON OF REPRESENTATIVE LOWER LIMB EXOSKELETON CONTROL PARADIGMS

Method	Gait phase detection	Parameter tuning	Power-based regulation
FSM [10], [11]	Yes	Yes	No
DOFC [12], [13]	No	Often	No
Optimization [1]	No	Yes	No
Learning [14]–[17]	No	No	No
Proposed (EGC)	**No**	**No**	**Yes**

not part of the control objective, and power regulation is used solely as a safety constraint rather than as a means of shaping task-level assistance.

Inspired by the principle of energy consistency underlying the safety considerations in collaborative arms [18], but extending beyond their original scope, we propose the energy-gated controller (EGC), a method that regulates exoskeleton assistance based on joint-level mechanical power so that positive assistive torque is delivered only during phases of positive joint work. Using two inertial measurement units (IMUs) as inputs and a small set of physically interpretable parameters, EGC operates across tasks, gait transitions, and subjects without parameter retuning.

The contribution of this article is a control method that achieves predominantly positive assistive mechanical power by regulating assistance directly using joint-level mechanical power rather than predefined gait phases or task modes. By treating mechanical power as a controlled variable instead of a secondary outcome of torque scheduling, the method promotes nonresistive interaction across locomotion conditions. EGC uses a two-module architecture: Module 1 (energy gate) permits torque only during predicted positive-power phases, and Module 2 (torque synthesis) reconstructs full-cycle assistance from a delayed and scaled flexion component. EGC operates without explicit gait-phase detection in real-time control, activity recognition, or manual parameter tuning, using only a small set of physically interpretable parameters.

II. ALGORITHM OF ASSISTIVE CONTROL

We present the algorithm of our controller below. Two thigh-mounted IMUs measure the sagittal-plane thigh angle and angular velocity, denoted $\theta_j^{\mathrm{IMU}}(t)$ and $\omega_j^{\mathrm{IMU}}(t)$, where $j \in \{L, R\}$ is the side index used throughout. These signals serve as low-dimensional proxies for hip motion and are not direct anatomical joint measurements. For simplicity, we use $\theta_j(t)$ and $\omega_j(t)$ to denote the filtered quantities derived from these measurements. Consistent with the system-level architecture, as shown in Fig. 1(a), the controller first processes IMU signals into predicted mechanical power P_j^{pred} and a pregating torque signal τ_j^{raw}. Module 1 (energy gate) then modulates τ_j^{raw} according to P_j^{pred} to produce τ_j^{gate}, and Module 2 (torque synthesis) constructs the final command τ_j^{sum}. Each symbol is formally defined in the subsections below; the internal signal flows of Modules 1 and 2 are illustrated in Fig. 2. The controller runs at 100 Hz with sampling interval $T_s = 10$ ms.

A. Module 1: Energy Gate

We define a relative leg-phase signal to capture the interlimb phase difference

$$\mathrm{RL}(t) \triangleq \theta_R(t) - \theta_L(t) \tag{1}$$

where $\theta_j(t)$ is obtained by applying a causal first-order low-pass filter $\mathcal{L}\{\cdot\}$ to the raw IMU measurement

$$\theta_j(t) = (1-\beta)\,\theta_j(t-1) + \beta\,\theta_j^{\mathrm{IMU}}(t) \tag{2}$$

where $\beta \in (0, 1)$ is the filter coefficient that determines the smoothing strength. A positive $\mathrm{RL}(t)$ indicates that the right leg is leading (i.e., in extension while the left leg is in flexion).

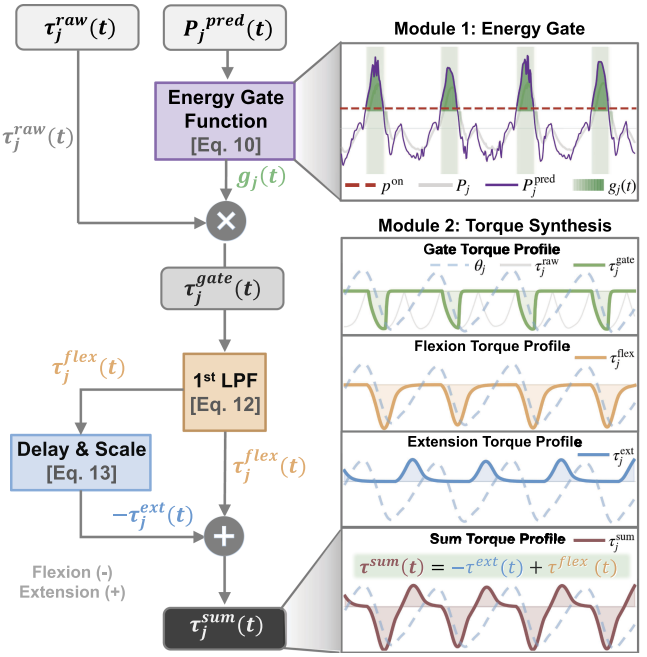

Fig. 2. Block diagram and representative signal waveforms of the EGC. Module 1 (energy gate) opens the gate only when predicted mechanical power exceeds the threshold, suppressing torque during negative-power phases. Module 2 (torque synthesis) smooths the gated torque to obtain the flexion component, then delays and scales it to form the extension component. The right panels show how each signal evolves through the two modules.

To align assistance timing, $\mathrm{RL}(t)$ is phase-shifted by a time offset Δt, producing the delayed phase signal

$$\mathrm{RL}^{\mathrm{dly}}(t) \;=\; \mathrm{RL}(t - \Delta t_i). \tag{3}$$

To maintain a consistent phase offset relative to the interlimb crossing, the total delay comprises an explicit term $\alpha\, T_i$ and the implicit group delay of Δt^{LPF} from the low-pass filter $\mathcal{L}\{\cdot\}$ in (2)

$$\Delta t_i \;=\; \alpha\, T_i \;+\; \Delta t^{\mathrm{LPF}} \tag{4}$$

where subscript i denotes the ith detected interlimb crossing, used consistently below, and T_i is the corresponding crossing interval

$$T_i = t_i - t_{i-1} \tag{5}$$

with t_i the timestamp of crossing i. Crossings are identified by a hysteretic zero-crossing detector on $\mathrm{RL}(t)$: given a threshold $h = 3^\circ$, a crossing is registered at time t_i when

$$\mathrm{RL}(t_i - T_s) \;\le\; -h \quad \text{and} \quad \mathrm{RL}(t_i) \;\ge\; +h. \tag{6}$$

Following [12], where a total offset of approximately 40% of the stride interval was shown to yield favorable assistance timing at walking speeds, we extend this principle to all alternating leg locomotion. With $\beta = 0.1$, the group delay of $\mathcal{L}\{\cdot\}$ is approximately $(1-\beta)/\beta = 9$ samples, i.e., $\Delta t^{\mathrm{LPF}} \approx 90$ ms ($\approx 0.09\, T_i$ at typical walking cadence). We therefore set $\alpha = 0.3$, giving a total offset $\Delta t_i \approx 0.4\, T_i$ at walking speeds. This value is kept fixed across all conditions as a conservative engineering choice, and residual timing mismatches are handled by *energy gate function* (10), which suppresses any torque that falls outside positive-power phases.

We generate side-specific pregating torque signals by assigning each hip a phase sensitive sign pattern. Let

$$\phi(t) \;=\; \mathrm{RL}^{\mathrm{dly}}(t)$$

denote the delayed relative leg phase. The raw pregating torque signal is

$$\tau_j^{\mathrm{raw}}(t) \;=\; s_j \begin{cases} -\,\phi(t), & \phi(t) \ge 0 \\ \phi(t), & \phi(t) < 0 \end{cases} \tag{7}$$

where $s_L = +1,\ s_R = -1$.

A. Gating via Predicted Power: A key contribution of this work is the introduction of *energy gate*, which restricts assistance to phases in which the exoskeleton performs positive mechanical work. Instantaneous mechanical power is estimated for each leg as the product of the raw pregating torque signal and the IMU-derived joint angular velocity

$$P_j(t) \;=\; \tau_j^{\mathrm{raw}}(t)\, \omega_j(t). \tag{8}$$

Power gating applies control effort only during assistive-work intervals, thereby reducing phases in which the commanded torque would oppose joint motion.

To compensate for perception–actuation latency, we apply a short-horizon linear extrapolation of the leg power over a lead time Δt^{lead}

$$P_j^{\mathrm{pred}}(t) \;=\; P_j(t) + \underbrace{\frac{P_j(t) - P_j(t - T_s)}{T_s}}_{\dot{P}_j(t)} \Delta t^{\mathrm{lead}} \tag{9}$$

where $\Delta t^{\mathrm{lead}} = \gamma\, T_i$. In this work, we set $\gamma = 0.06$, i.e., 6% of the crossing interval. The finite-difference derivative term $\dot{P}_j(t)$ is softly limited in magnitude to suppress high-frequency noise and prevent overshoot. The predicted power $P_j^{\mathrm{pred}}(t)$ is then used in the gating function (10) to anticipate the onset of positive mechanical work.

To selectively enable assistance during positive-work intervals, we define the *energy gate function* for each leg

$$g_j(t) \;=\; \frac{1}{2}\Big[\tanh\Big(k\,\Big(P_j^{\mathrm{pred}}(t) - p^{\mathrm{on}}\Big)\Big) + 1\Big]. \tag{10}$$

The gate $g_j(t) \in [0, 1]$ continuously modulates the pregating torque using the predicted power P_j^{pred} obtained above, together with two parameters: the activation threshold p^{on} and the transition sharpness k. When $P_j^{\mathrm{pred}} \ll p^{\mathrm{on}}$, $g_j \approx 0$ and assistance is fully suppressed, when $P_j^{\mathrm{pred}} \gg p^{\mathrm{on}}$, $g_j \approx 1$ and the full torque is delivered.

In our implementation, $p^{\mathrm{on}} = 5$ is set near the lower bound of the observed positive-power range so that the gate retains the majority of positive-power intervals while rejecting near-zero noise, ensuring activation even at slow walking speeds. The steepness $k = 5$ yields a smooth transition band over $P_j^{\mathrm{pred}} \in [3, 7]$, providing sufficient margin against fluctuations. Both values were fixed from pilot walking data and kept constant across all subjects, speeds, and tasks. A post hoc check confirmed

that varying p^{on} within $[5, 8]$ shifts gate duty by less than 3.5% without altering speed-scaling trends.

Finally, Module 1 produces a gated torque signal, in which only the portions corresponding to positive mechanical work are retained. This signal is then passed to Module 2 for full-cycle torque synthesis via delayed replication

$$\tau_j^{\text{gate}}(t) \;=\; g_j(t)\,\tau_j^{\text{raw}}(t). \tag{11}$$

Because both $|\tau_j^{\text{raw}}|$ and the gate duty g_j increase with locomotion speed, the gated assistance scales up naturally without any speed-dependent parameter adjustment.

B. Module 2: Biomechanics-Informed Torque Synthesis

After Module 1 gating, we obtain per-leg gated torque signals $\tau_j^{\text{gate}}(t)$. Rather than prescribing an independent full-cycle assistive waveform (e.g., sinusoid or oscillator), EGC constructs the extension component as a delayed, sign-inverted replica of the flexion torque. The gated signal is first smoothed by the same first-order filter (2) to obtain the *flexion-dominant* assistance component

$$\tau_j^{\text{flex}}(t) \;=\; \mathcal{L}\Big\{\tau_j^{\text{gate}}(t)\Big\}. \tag{12}$$

To provide bidirectional assistance, a bioinspired *phase-replication module* mirrors the flexion torque with a fixed delay and a scaling gain. The extension torques are given by

$$\tau_j^{\text{ext}}(t) \;=\; -g^{\text{ext}}\,\tau_j^{\text{flex}}\big(t-\Delta t^{\text{ext}}(t)\big) \tag{13}$$

where $g^{\text{ext}} \geq 0$ denotes the extension gain and $\Delta t^{\text{ext}}(t)$ is the replication delay applied to the low-pass-filtered flexion torque. In this work, we set

$$\Delta t^{\text{ext}}(t) = 0.45\,T_i, \qquad g^{\text{ext}} = 0.5$$

with T_i the instantaneous crossing interval from Module 1.

Previous studies placed hip extension assistance anywhere from early stance (10%–15%) to late stance (50%–60%) of the gait cycle [21]. Since the first-order filter additionally contributes a group delay of $\Delta t^{\text{LPF}} \approx 90$ ms, the effective extension timing shifts further into stance. Accounting for this offset, we set $\Delta t^{\text{ext}}(t) = 0.45\,T_i$ a priori to place extension assistance within the reported beneficial range. This value was determined before formal experiments and held fixed across all subjects, tasks, and speeds; the cross-condition results in Section IV confirm that this fixed choice provides consistent assistance without per-condition tuning.

The extension gain is set to $g^{\text{ext}} = 0.5$ for two reasons. First, hip extension primarily provides auxiliary support compared to ankle-driven propulsion [22], [23]. Second, excessive extension torque during stance can interfere with natural limb dynamics [11], [23]. This conservative, fixed gain was used across all subjects, tasks, and speeds without adjustment.

The final per-leg torque sums the flexion main channel and its delayed replica for extension

$$\tau_j^{\text{sum}}(t) = \underbrace{\tau_j^{\text{flex}}(t)}_{\text{flexion main channel}} + \underbrace{\big(-g^{\text{ext}}\big)\,\tau_j^{\text{flex}}\big(t-\Delta t^{\text{ext}}(t)\big)}_{\text{delayed replica for extension}}. \tag{14}$$

III. Experiments

As described in Section II, the EGC comprises five parameters, all determined a priori and held constant across all subjects, tasks, and speeds

$$\begin{aligned} \alpha = 0.3, \qquad p^{\text{on}} = 5, \qquad k = 5 \\ g^{\text{ext}} = 0.5, \qquad \Delta t^{\text{ext}}(t) = 0.45\,T_i. \end{aligned} \tag{15}$$

No parameters were retuned in any of the experiments reported in this article. Six participants ($n = 6$) were recruited, consistent with prior exoskeleton studies evaluating control algorithms [21].

We evaluate the EGC in two experiments to examine whether a single fixed parameter set can maintain positive power assistance across different speeds, subjects, and tasks: 1) periodic treadmill gait at five speeds (0.75–3.5 m/s), including comparison with a benchmark controller, and 2) five nonperiodic overground locomotion tasks covering speed changes and task transitions.

During all experiments, two IMUs were mounted on the thigh bars for real-time control, and one IMU was attached to the dorsal side of each foot for offline gait-event labeling only, as shown in Fig. 3(b). Gait-cycle boundaries were identified from the minima of the dorsal-foot angle signal, which approximately correspond to heel strikes (HS) [24], [25]. Four gait events: HS, foot-flat (FF), heel-off (HO), and toe-off (TO) were then detected from the dorsal-foot angular-velocity profiles following [26], as illustrated in Fig. 3(a). All participants provided written informed consent prior to participation.

For evaluation, a customized load cell (LZ-NJ60/97.5/10, Hefei Lizhi Sensor Systems Co., Ltd., China) was installed between the motor gearbox output and the thigh linkage, directly measuring the actuator output torque τ_j^{meas}. The load-cell full scale (F.S.) is 40 N·m; the specification-based static torque uncertainty estimate is approximately $\pm 1.5\%$F.S. (± 0.60 N·m), and the nominal resolution is 0.04 N·m. Mechanical power was computed as

$$P_j^{\text{meas}}(t) = \tau_j^{\text{meas}}(t)\,\omega_j(t) \tag{16}$$

where $\omega_j(t)$ is the IMU-derived thigh angular velocity. This quantity represents the mechanical power delivered by the exoskeleton actuator. For visualization, load-cell signals were post-processed with a zero-phase second-order Butterworth low-pass filter at 6 Hz to remove measurement noise. All assistive torque and power values reported in the experimental results are derived from load-cell measurements.

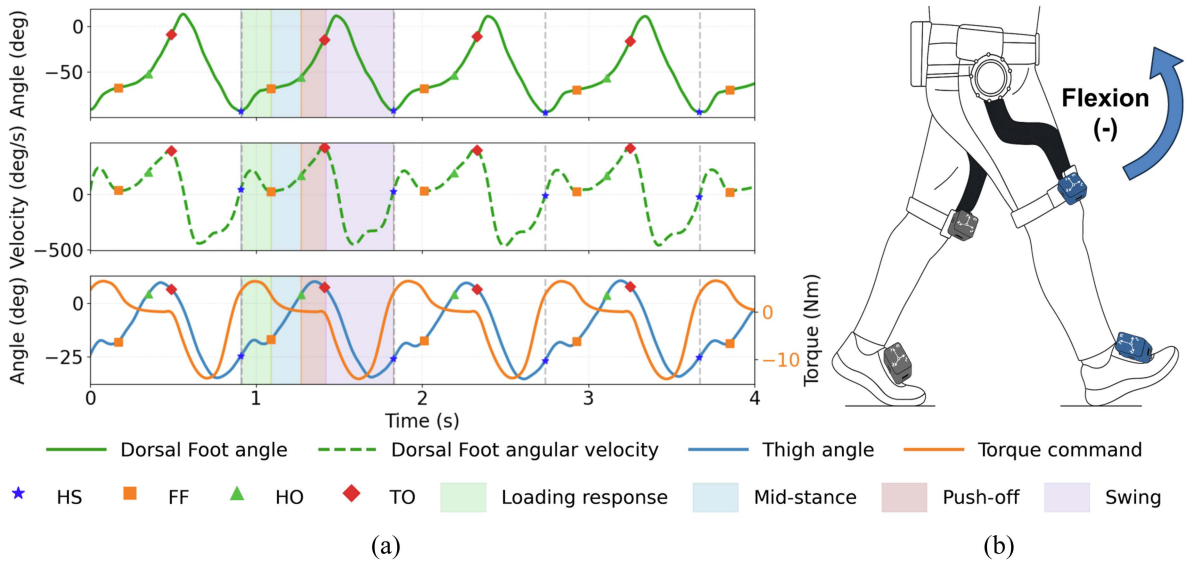

Fig. 3. (a) Offline gait segmentation at 1.75 m/s. From top to bottom: dorsal-foot angle, dorsal-foot angular velocity, and thigh angle (IMU-derived hip-motion proxy) with the corresponding torque command. Gait-cycle boundaries were identified from dorsal-foot angle minima [24], [25], and four gait events (HS, FF, HO, and TO) were detected from the angular-velocity signal [26]. Colored regions indicate gait phases. (b) IMU placement. Thigh-mounted IMUs provide real-time inputs to the controller; foot-mounted IMUs are used exclusively for offline gait-event labeling.

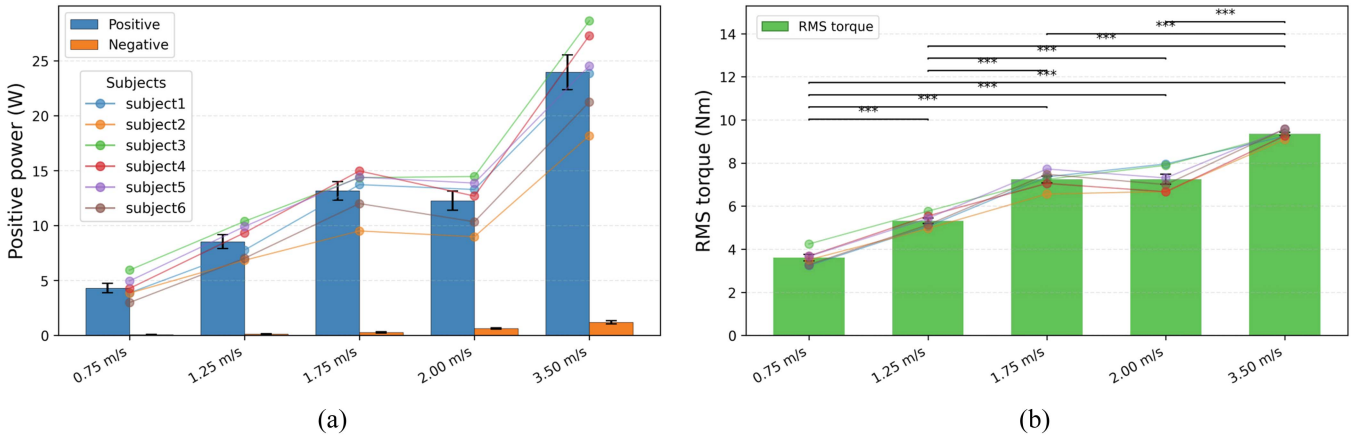

Fig. 4. Performance of the EGC across locomotion speeds ($n = 6$). (a) Mean positive (blue) and negative (orange) mechanical power per leg. Bars indicate group mean $\pm$ SD; colored lines show individual subjects. Positive power increases with speed while negative power remains near zero at all speeds. (b) RMS assistive torque at each speed. Colored lines show individual subjects. RMS torque increases with speed while intersubject variability remains low. One-way analysis of variance with post hoc pairwise tests: $^{*}p < 0.05$, $^{**}p < 0.01$, and $^{***}p < 0.001$.

A. Experiment 1: Periodic Gait Across Speeds and Subjects

Participants: Six healthy adults (four males and two females) participated in this experiment. The participants' demographics were as follows: age, 23.0 $\pm$ 2.1 years; weight, 65.3 $\pm$ 14.2 kg; height, 174.5 $\pm$ 6.5 cm [mean $\pm$ standard deviation (SD)]. All participants had prior experience using the exoskeleton.

Protocol: Participants evaluated the EGC and a benchmark controller using a randomized crossover design across five speeds (0.75, 1.25, 1.75, 2.0, and 3.5 m/s). Both the controller assignment and the speed sequences were randomized for each subject, with 3 min rest intervals between consecutive trials. For each speed, data from the middle 30 gait cycles were extracted.

1) Analysis of Assistive Energy Delivery: Fig. 4(a) shows the mean per-cycle mechanical power. Across all five speeds, including running at 2.0 and 3.5 m/s, the delivered positive power increases with speed while the negative power remains near zero, indicating that the EGC delivers positive mechanical work at every tested condition with minimal negative-power components. Intersubject variability is low, as shown by the individual subject traces.

Fig. 4(b) reports the root mean square (RMS) assistive torque across speeds. The torque magnitude increases significantly from 0.75 to 3.5 m/s (all pairwise comparisons $p < 0.001$), while intersubject variability remains small despite the use of a single

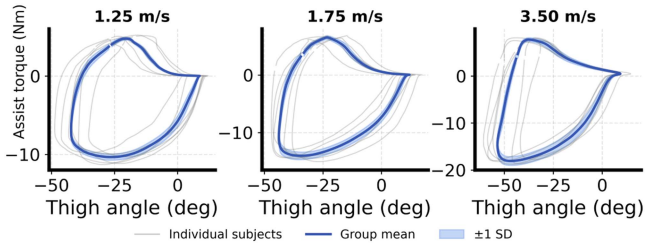

Fig. 5. Torque-angle loops of the EGC across three locomotion speeds ($n = 6$). Gray curves: individual subjects (30-cycle average each); blue curve: group mean; shading: ± 1 SD. In such loops, clockwise enclosed area corresponds to net positive work delivered to the user, while self-intersections create counterclockwise subloops that indicate negative work phases where the exoskeleton opposes joint motion. Across all speeds, both individual and group-mean EGC loops remain smooth and clockwise with negligible self-intersections.

fixed parameter set. This emergent scaling is consistent with the gating mechanism: as speed increases, both $|\tau_j^{\text{raw}}|$ and the gate duty increase [see. (10) and (11)], yielding larger gated torque without speed-specific gain scheduling.

2) Torque-Angle Loop Analysis: Torque-angle loops directly reflect the mechanical work exchanged between the exoskeleton and the human joint [27]. Following established practice, we assess three geometric features: *loop consistency* across subjects and cycles, indicating a repeatable energy-exchange pattern [27]; *clockwise traversal*, corresponding to net positive work delivered by the exoskeleton [28]; and *minimal self-intersections*, as loop reversals or figure-eight patterns indicate phases where assistive torque opposes joint motion [29].

Fig. 5 shows the torque-angle loops at three representative speeds. At the individual subject level (gray curves), all six participants exhibit smooth, closed, and consistently clockwise loops with negligible self-intersections across both walking and running. The narrow ± 1 SD band around the group mean further confirms low intersubject variability in loop morphology. These results indicate that the power-based gating produces net positive mechanical work with consistent phase alignment across subjects and speeds, without speed-specific tuning.

3) Comparison With Benchmark Controller: Fig. 6 presents a subject-matched head-to-head comparison between the EGC and a benchmark controller under identical experimental conditions. The EGC uses the same fixed parameter set at all speeds, whereas the benchmark uses speed-dependent parameters, as detailed in Fig. 6. The EGC torque-angle loops remain smooth and clockwise across all speeds. In contrast, the benchmark loops develop visible self-intersections at higher speeds, indicating increased negative-work phases.

Fig. 7 quantifies this difference. Across all six subjects and speeds (0.75–3.5 m/s), the EGC achieved positive-power ratios of 97.8%–98.4% during walking and 94.8%–95.1% during running, all obtained with the fixed parameter set. The benchmark achieved 91.7%–93.7% during walking and 86.5%–87.3% during running, using speed-dependent parameters. The bottom row of Fig. 6 further shows that the EGC mechanical power remains predominantly positive across the gait cycle at all

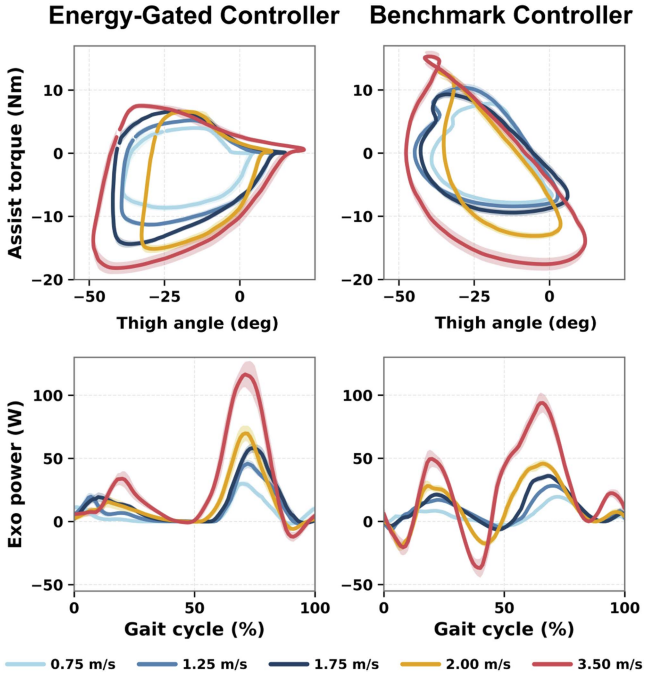

Fig. 6. Representative head-to-head comparison between the proposed EGC and a benchmark controller. Top row: assistive torque plotted against IMU-derived thigh angle (hip-motion proxy). Bottom row: corresponding exoskeleton mechanical power over the gait cycle. EGC is evaluated using a single fixed parameter set across all subjects, tasks, and speeds without retuning. The benchmark controller is evaluated using speed-dependent parameters reported in prior work: $\Delta t = 0.25$ s and $\kappa = 10$ for 0.75–1.75 m/s [12], and $\Delta t = 0.20$ s and $\kappa = 20$ for 2.00 and 3.50 m/s [13]. The plots show the resulting torque-angle loops and mechanical power profiles for both controllers.

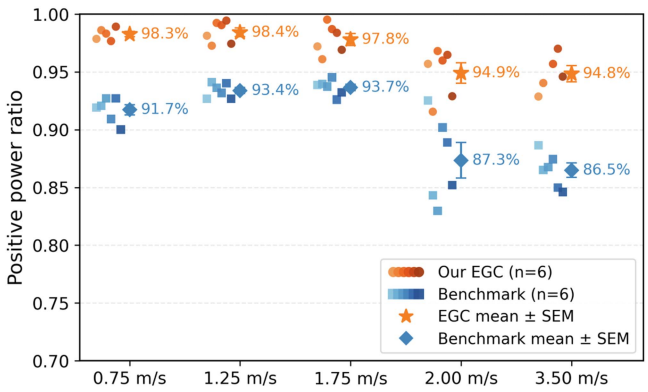

Fig. 7. Positive mechanical power ratio of the EGC and the benchmark controller ($n = 6$). EGC results show the group mean $\pm$ standard error of the mean using a single fixed parameter set. Benchmark data are from the same cohort under identical conditions with speed-dependent parameters [12], [13].

speeds, whereas the benchmark exhibits notable negative-power intervals at 2.0 and 3.5 m/s.

These results highlight the practical benefit of conditioning actuation directly on predicted joint power flow. Because the energy gate continuously evaluates whether the joint is performing positive work, assistance timing adapts to the underlying

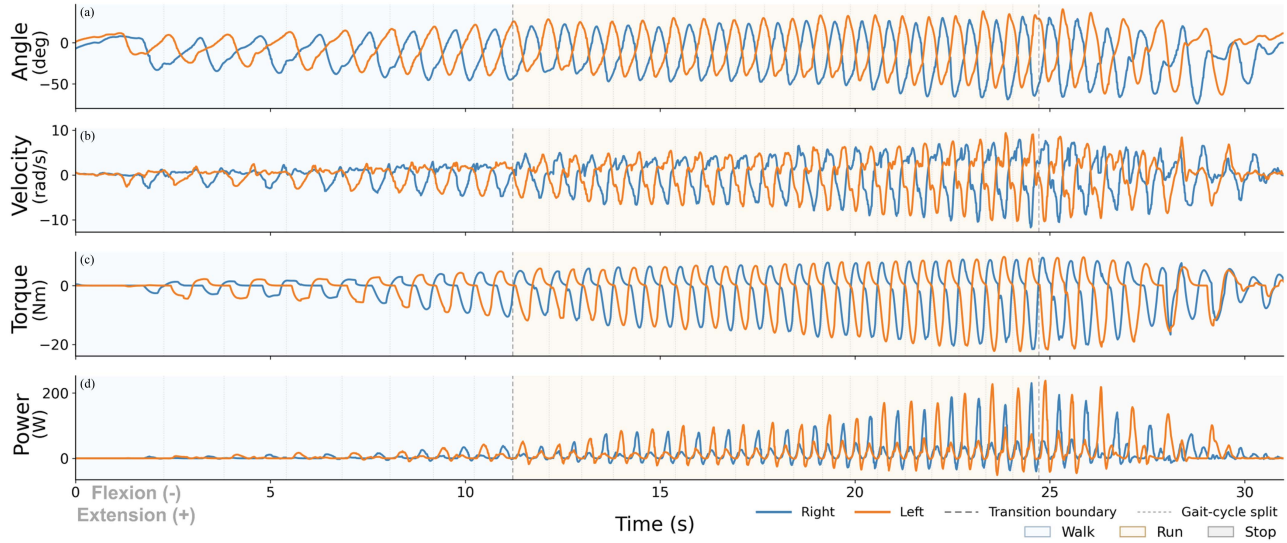

Fig. 8. Continuous speed transition from walking through running and then decelerating toward a near-stop. (a) Thigh angle. (b) Angular velocity. (c) Assistive torque. (d) Mechanical power. The dashed vertical lines mark the walk-to-run transition (around 11 s) and the onset of deceleration (around 25 s). Torque and power in (c) and (d) evolve continuously across both transitions without discontinuities or sign inversions; the gate progressively closes during deceleration.

gait dynamics without requiring speed-specific or task-specific parameters. The resulting positive power ratios remain consistently high across the entire tested speed range with a single fixed parameter set.

B. Experiment 2: Nonperiodic Locomotion and Gait Transitions

The energy gate continuously evaluates predicted joint power, independently of locomotion type. No task classifier, gait template, or mode switching is involved. Assistance is delivered whenever the joint performs positive work and suppressed otherwise. This allows the same fixed parameter set to operate across fundamentally different locomotion tasks without reconfiguration. To test this directly, we evaluate the EGC during five nonperiodic overground tasks that include transitions between walking, running, stopping, and stair climbing.

Five tasks were conducted: three stop-and-go tasks (walk–stop–walk, run–stop–run, and run–stop–walk), a continuous speed transition from walking through running and then decelerating toward a near-stop state, and stair climbing. Since walk–stop–walk and run–stop–run are subsets of run–stop–walk, we present three representative tasks as follows.

Walk-to-run-to-stop transition: The speed was continuously increased from walking to running and then decreased toward a near-stop state, requiring the participant to adapt across the full speed range. As shown in Fig. 8(c) and (d), the assistive torque and mechanical power evolve continuously across the walk-to-run transition without discontinuities or sign inversions. During deceleration, the predicted power decreases and the energy gate progressively closes, reducing assistance naturally.

Run–stop–walk: The participant ran, came to a complete stop, and then resumed walking. As shown in the right column of Fig. 9, the energy gate suppressed torque and power during the stop phase as predicted power fell below p^{on}, and re-engaged assistance once walking resumed and positive power reappeared.

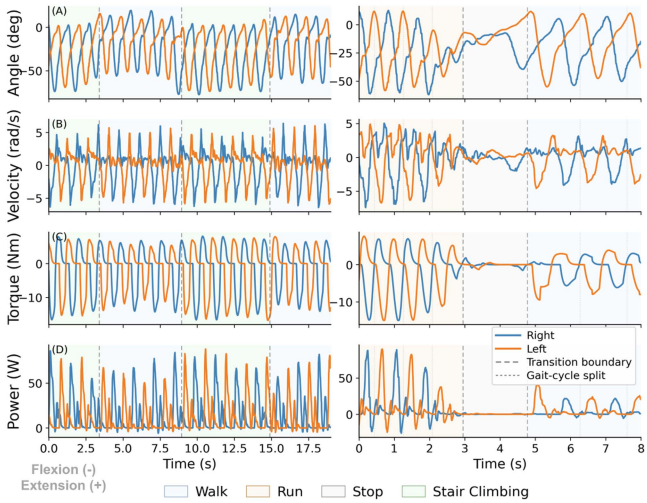

Fig. 9. Nonperiodic locomotion tasks. Left column: stair climbing, with transitions between level walking and stair ascent/descent. Right column: run–stop–walk. Each column shows, from top to bottom. (a) Thigh angle. (b) Angular velocity. (c) Assistive torque. (d) Mechanical power. In both tasks, torque and power drop to near zero during stopping or low-power intervals and recover when positive-power locomotion resumes.

Real-world stair climbing: This task was performed on an actual staircase, with alternating stair ascent, level walking between floors, and stair descent. The left column of Fig. 9 shows that the EGC adapted torque magnitude and timing across these transitions without any task-specific mode or parameter change.

Across all five tasks, which cover speed changes, gait-type transitions, complete stops, and stair climbing, the energy gate delivered assistance during positive-power phases and suppressed it when predicted power dropped, without any task

classifier, mode switch, or parameter adjustment. Combined with Experiment 1, these results demonstrate that a single fixed parameter set can maintain positive-power assistance across subjects, speeds, locomotion tasks, and gait transitions.

IV. Discussion

A. Mechanistic Interpretation Across Periodic and Nonperiodic Motions

EGC combines two fixed modules to shape assistance under a single parameter set. Module 1 gates assistance using predicted joint mechanical power, so assistance is attenuated when positive-work conditions are not met. Module 2 synthesizes full-cycle torque by delayed, scaled replication of the flexion component. Because gating is driven by real-time power flow rather than discrete task or mode switching, torque timing and magnitude vary continuously with speed changes and gait transitions (see Figs. 4 and 8). These observations are consistent with the high positive-power ratios reported in Section III.

The emergent torque–speed scaling, as observed in Fig. 4(b), can be traced to the gating mechanism. As locomotion speed increases, both the magnitude and duration of positive-power intervals grow, so the effective gated torque signal increases without explicit gain scheduling, consistent with the monotonic RMS torque increase across 0.75–3.5 m/s ($p < 0.001$). The gate saturation ($g_j \to 1$ when $P_j^{\text{pred}} \gg p^{\text{on}}$) provides a natural upper bound, as reflected by the diminishing torque increment at the highest speeds. Meanwhile, Fig. 4(a) confirms that positive power grows with speed while negative power remains near zero, indicating selective amplification of positive-work phases. Experiment 2 further shows that the same mechanism extends to nonperiodic motions: the gate opens and closes in response to instantaneous power flow without task classification or mode switching.

From a design perspective, the proposed EGC differs from existing exoskeleton control methods in its choice of regulated variable. Conventional approaches, whether FSM-based, delayed-output feedback, optimization-based, or learning-based, generate assistive torque from kinematic phase, delayed feedback, or learned policies, where the sign of mechanical power at the joint is a downstream consequence rather than an explicit control input. EGC conditions actuation directly on predicted joint power flow, making positive-work delivery a design objective within the control loop.

B. Limitations and Future Work

First, this study focused on controller-level evaluation using kinematic and kinetic measures, which directly reflect whether the energy gate delivers assistance during positive-power phases as intended. Metabolic cost is a complementary outcome and will be quantified in future studies.

Second, all five parameters were selected a priori and held fixed across subjects, speeds, and tasks throughout the experiments. At the highest running speed, small residual negative-power lobes remain due to rapid kinematic changes and finite sensing-actuation latency, suggesting headroom for adaptive parameter strategies. Perturbation cases, such as stumble recovery, where both legs may move in a more symmetric pattern, were not tested and warrant future investigation.

Third, assistive torque was measured at the actuator output via a load cell, which provides a direct and repeatable basis for evaluating the control law. Instrumenting the human–exoskeleton contact interface would further extend the analysis to interaction biomechanics and is planned for future work.

V. Conclusion

This article presented the EGC, which conditions hip exoskeleton assistance directly on predicted joint power flow using two thigh-mounted IMUs and five fixed parameters. Across six participants and a continuous speed range of 0.75–3.5 m/s, EGC maintained over $97.8\% \pm 1.2\%$ positive mechanical power in walking and above $94.8\% \pm 1.6\%$ in running, without task-specific or speed-specific retuning. The same parameter set operated across five nonperiodic locomotion tasks, including speed transitions, stop-and-go, and stair climbing, without task classification or mode switching. These results demonstrate that regulating assistance through joint-power flow provides a practical and effective design principle for multispeed, multitask hip exoskeleton control.

References

[1] Y. Ding, M. Kim, S. Kuindersma, and C. J. Walsh, "Human-in-the-loop optimization of hip assistance with a soft exosuit during walking," *Sci. Robot.*, vol. 3, no. 15, 2018, Art. no. eaar5438.

[2] S. Maggioni, L. Lünenburger, R. Riener, A. Curt, M. Bolliger, and A. Melendez-Calderon, "Assessing walking ability using a robotic gait trainer: Opportunities and limitations of assist-as-needed control in spinal cord injury," *J. NeuroEng. Rehabil.*, vol. 20, no. 1, 2023, Art. no. 121.

[3] B. Lim, B. Choi, C. Roh, J. Lee, Y. J. Kim, and Y. Lee, "Ultra-lightweight robotic hip exoskeleton with anti-phase torque symmetry for enhanced walking efficiency," *Sci. Rep.*, vol. 15, no. 1, 2025, Art. no. 10850.

[4] S. Yu et al., "Quasi-direct drive actuation for a lightweight hip exoskeleton with high backdrivability and high bandwidth," *IEEE/ASME Trans. Mechatron.*, vol. 25, no. 4, pp. 1794–1802, Apr., 2020.

[5] T. G. Sugar, E. Fernandez, D. Kinney, K. W. Hollander, and S. Redkar, "HeSA: Hip exoskeleton for superior assistance," in *Proc. Wearable Robot.: Challenges Trends*, 2016, pp. 319–323.

[6] S. A. Murray, K. H. Ha, C. Hartigan, and M. Goldfarb, "An assistive control approach for a lower-limb exoskeleton to facilitate recovery of walking following stroke," *IEEE Trans. Neural Syst. Rehabil. Eng.*, vol. 23, no. 3, pp. 441–449, Mar., 2014.

[7] R. Baud, A. R. Manzoori, A. Ijspeert, and M. Bouri, "Review of control strategies for lower-limb exoskeletons to assist gait," *J. NeuroEng. Rehabil.*, vol. 18, no. 01, 2021, Art. no. 119.

[8] C. Siviy et al., "Opportunities and challenges in the development of exoskeletons for locomotor assistance," *Nat. Biomed. Eng.*, vol. 7, no. 4, pp. 456–472, 2023.

[9] D. Rodriguez-Jorge et al., "Biomechanics-informed mechatronics design of comfort-centered portable hip exoskeleton: Actuator, wearable interface, controller," *IEEE Trans. Med. Robot. Bionics*, vol. 7, no. 2, pp. 687–698, May 2025.

[10] J. Jang, K. Kim, J. Lee, B. Lim, and Y. Shim, "Online gait task recognition algorithm for hip exoskeleton," in *Proc. IEEE/RSJ Int. Conf. Intell. Robots Syst. (IROS)*, 2015, pp. 5327–5332.

[11] K. Seo, S. Hyung, B. K. Choi, Y. Lee, and Y. Shim, "A new adaptive frequency oscillator for gait assistance," in *Proc. IEEE Int. Conf. Robot. Automat. (ICRA)*, 2015, pp. 5565–5571.

[12] B. Lim et al., "Delayed output feedback control for gait assistance with a robotic hip exoskeleton," *IEEE Trans. Robot.*, vol. 35, no. 4, pp. 1055–1062, Apr., 2019.

[13] B. Lim, B. Choi, C. Roh, S. Hyung, Y.-J. Kim, and Y. Lee, "Parametric delayed output feedback control for versatile human-exoskeleton interactions during walking and running," *IEEE Robot. Autom. Lett.*, vol. 8, no. 8, pp. 4497–4504, Aug., 2023.

[14] S. Luo et al., "Experiment-free exoskeleton assistance via learning in simulation," *Nature*, vol. 630, no. 8016, pp. 353–359, 2024.

[15] Y. Zhou et al., "A simulation-based lower-limb exoskeleton control method," in *Proc. IEEE Int. Conf. Robot. Biomimetics* (ROBIO), Dec. 2025, pp. 1453–1458.

[16] I. Park, C. Song, and I. Kang, "Learning hip exoskeleton control policy via predictive neuromusculoskeletal simulation," 2026, *arXiv:2603.04166*.

[17] M. Kim, W.-J. Baek, and J. Park, "A deep reinforcement learning-based end-to-end control framework for lower-limb exoskeletons with smooth movement transitions," in *Proc. IEEE/RSJ Int. Conf. Intell. Robots Syst. (IROS)*, Oct. 2025, pp. 12005–12012.

[18] P. Aivaliotis, S. Aivaliotis, C. Gkournelos, K. Kokkalis, G. Michalos, and S. Makris, "Power and force limiting on industrial robots for human-robot collaboration," *Robot. Comput.- Integr. Manuf.*, vol. 59, pp. 346–360, Oct. 2019.

[19] A. Dietrich, X. Wu, K. Bussmann, C. Ott, A. Albu-Schäffer, and S. Stramigioli, "Passive hierarchical impedance control via energy tanks," *IEEE Robot. Autom. Lett.*, vol. 2, no. 2, pp. 522–529, Feb., 2017.

[20] Y. Yan et al., "Compact and foldable hip exoskeleton with high torque density actuator for walking and stair-climbing assistance in young and older adults," *IEEE/ASME Trans. Mechatron.*, pp. 1–11, 2025.

[21] M. Grimmer et al., "Comparison of the human-exosuit interaction using ankle moment and ankle positive power inspired walking assistance," *J. Biomech.*, vol. 83, pp. 76–84, 2019.

[22] D. A. Winter, "The Biomechanics and Motor Control of Human Gait," Waterloo, ON, Canada: Univ. Waterloo, 1987.

[23] J. M. Donelan, R. Kram, and A. D. Kuo, "Mechanical work for step-to-step transitions is a major determinant of the metabolic cost of human walking," *J. Exp. Biol.*, vol. 205, no. 23, pp. 3717–3727, 2002.

[24] S. P. Kwakkel, S. Godha, and G. Lachapelle, "Foot and ankle kinematics during gait using foot mounted inertial system," in *Proc. Nat. Tech. Meeting Inst. Navigation*, Jan. 2007, pp. 1056–1064.

[25] C. Voisard, N. De l'Escalopier, D. Ricard, and L. Oudre, "Automatic gait events detection with inertial measurement units: Healthy subjects and moderate to severe impaired patients," *J. NeuroEng. Rehabil.*, vol. 21, no. 1, 2024, Art. no. 104.

[26] H. Zhao, Z. Wang, S. Qiu, Y. Shen, and J. Wang, "IMU-based gait analysis for rehabilitation assessment of patients with gait disorders," in *Proc. 4th Int. Conf. Syst. Informat. (ICSAI)*, Nov. 2017, pp. 622–626.

[27] H. Lee and N. Hogan, "Time-varying ankle mechanical impedance during human locomotion," *IEEE Trans. Neural Syst. Rehabil. Eng.*, vol. 23, no. 5, pp. 755–764, May 2014.

[28] L. M. Mooney, E. J. Rouse, and H. M. Herr, "Autonomous exoskeleton reduces metabolic cost of human walking during load carriage," *J. NeuroEng. Rehabil.*, vol. 11, no. 1, 2014, Art. no. 80.

[29] J. Kim et al., "Reducing the metabolic rate of walking and running with a versatile, portable exosuit," *Sci.*, vol. 365, no. 6454, pp. 668–672, 2019.